Markerless Gait Classification Employing 3D IR-UWB Physiological Motion Sensing

Soumya Prakash Rana*, Maitreyee Dey, *Member, IEEE,* Mohammad Ghavami, *Senior Member, IEEE,* and Sandra Dudley, *Member, IEEE*

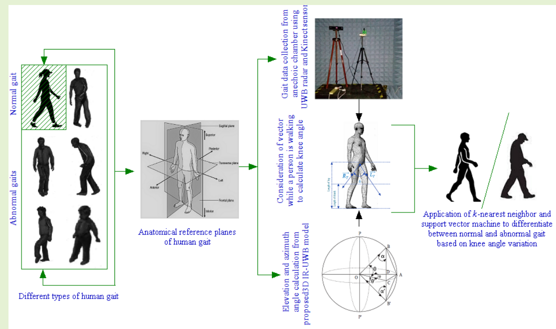

***Abstract*—Human gait refers to the propulsion achieved by the effort of human limbs, a reflex progression resulting from the rhythmic reciprocal bursts of flexor and extensor activity. Several quantitative models are followed by health professionals to diagnose gait abnormality. Marker-based gait quantification is considered a gold standard by the research and health com- munities. It reconstructs motion in 3D and provides parameters to measure gait. But, it is an expensive and intrusive technique, limited to soft tissue artefact, prone to incorrect marker positioning, and skin sensitivity problems. Hence, markerless, swiftly deployable, non-intrusive, camera-less prototypes would be a game changing possibility and an example is proposed here. This paper illustrates a 3D gait motion analyser employing impulse radio ultra-wide band (IR-UWB) wireless technology. The prototype can measure 3D motion and determine quantitative parameters considering anatomical reference planes. The knee angles have been calculated from gait by applying vector algebra. Simultaneously, the model has been corroborated with the popular markerless camera based 3D motion capturing system Kinect sensor. Bland and Altman (B&A) statistics has been measured between the proposed prototype and Kinect sensor results to verify the measurement agreement. Finally, the proposed prototype has been incorporated with popular supervised machine learning and deep learning techniques to automatically recognize gait abnormalities, with promising results presented.**

***Index Terms*—Gait, Impulse Radio Ultra-Wide Band (IR-UWB), Knee Angle Extraction, Kinect Xbox Sensor, Bland and Altman Plot, Machine Learning, Deep Multilayer Perceptron.**

I. Introduction

HUMAN gait motion is an association of several voluntary movements resulting from complex processes where the brain, spinal cord, muscles, nervous system, bones, and joints function together. Both the upper and lower limbs synchronize simultaneously in this translational process. Physically, each and every bone participates in the process, but empirically the bones of the pelvis and lower limbs are normally considered to realize this repetitive locomotion. The rudiments of three different disciplines, anatomy, physiology, and biomechanics are obligatory to appreciate movement. Anatomy of gait explains the relationships between different body parts based on their anatomical positions in the sagittal, frontal, and transverse planes [1]. The joint and associated muscle movements are further divided based on the movement direction in the reference planes, the movements are flexion-extension, abduction-adduction, and internal-external rotation. Gait physiology involves different nervous systems and signals transmitted or received from the relevant motor system, where this communication transforms into a motion. Biomechanics is a study of the skeletal muscle's (primarily responsible for gait) movements with the help of mechanical engineering to investigate quantitative gait parameters [2]. Gait parameters are predominantly used to practically measure lower limb movement in clinical assessment, where movement quality is analysed by anatomy and physiology. Pathological gait is realized when a person is unable to walk in the 'usual' way, due to collapsed support, leg complicacy, insufficient limb strength, trunk injury, arthritis, soft tissue infection, birth defects, cerebral palsy, stroke, etc. These problems are measured and monitored mainly for healthcare (e.g., Parkinson's disease), athletic performance, rehabilitation reasons, etc. Abnormalities are categorized into five types based on the range of symptoms such as, spastic, scissors, steppage, waddling, and propulsive gait, pictorially shown in Figure 1.

Authors are with Centre for Biomedical Engineering and Communications (BiMEC), London South Bank University, 103 Borough Road, London SE1 0AA, United Kingdom.

This work forms part of the project ROVER: Reliable Technologies and Models for Verified Wireless Body-Centric Transmission and Localization. Areas of the research has been funded by Research and Innovation Staff Exchange (H2020-MSCA-RISE-2019), Grant Agreement Number: 872752.

S. P. Rana is the corresponding author (Email: soumyaprakash.rana@gmail.com, ranas11@lsbu.ac.uk).

(a) Spastic (b) Scissor (c) Propulsive (d) Steppage (e) Waddle

Fig. 1: Types of abnormal gaits and reflections on individual's walk [3].

II. Diagnosis of Gait & State-of-Art Technologies

Quantitative gait assessment is an accepted and less error prone method due to the employment of advanced technical instruments beyond that of visual observation applied in qualitative monitoring in gait diagnosis. These technologies are classified into 2D and 3D models based on their ability to measure anatomical landmarks. The 2D quantitative models can measure gait parameters such as step, acceleration, speed, body orientation, angular velocity, magnetic field using inertial instruments, such as accelerometers, gyroscopes, magnetometers, etc. [4]. These parameters relate only to the sagittal and frontal planes which actually lack information regarding the postural aspect. Moreover, these are not standalone schemes but practised along with other clinical gait instruments. Clinical gait requires models and instruments that depict the required parameters as well as the body's appearance during movement to realize the overall, personalized mechanics of the musculoskeletal system. This can be addressed with a 3D motion capture (also known as '3D mocap') model adding an extra dimension i.e., transverse plane anatomy to the gait motion analysis which aims to assist professionals to more precisely understand both body appearance and gait biomechanics simultaneously.

There are two types of 3D mocap models, marker-based and markerless [5]. Video based optoelectronic techniques employ retro-reflective markers attached to the patient's body in marker-based models to reconstruct movement and identify anatomical landmarks in 3D. However, it faces the soft tissue artefact problem i.e., the abnormality related to bone is difficult to detect if the marker positions are incorrectly placed. Also, patients often suffer skin sensitivity issues from the adhesive tape and electrode markers used. Thus, markerless or non-contact 3D gait has gained increasing interest in the biomechanics and biomedical community. Conventional markerless 3D gait estimation is performed by employing multiple cameras or camera sensors to determine kinetics and kinematics [6]. The video data frames are synchronized from different view- points to reconstruct movement information. Currently, the biomechanics and biomedical communities collaborate with computer vision adopting conventional machine learning (ML) and deep learning (DL) to recognize gait abnormality. Viewing angle and frame synchronization maintenance are the most demanding tasks for this method. Markerless 3D gait models are classified into two further groups, model-free and model-based approaches. The model-free approaches use a likelihood function to identify joints, pose, and body shape whereas the model-based approaches use a priori knowledge of the human body to estimate gait. However, current model-free and model-based gait research exploiting ML generally focus on person identification and not to identify/diagnose walking abnormalities or disorders, and for identification, the wearable sensing tool is still the preferred research field in motion analysis [7] hitherto. These investigations largely make use of smartphone's inbuilt inertial sensors, accelerometers, and gyroscopes. For instance, Muaaz and Mayrhofer developed an android application employing smartphone accelerometers to analyse walking data to establish the identity of an individual in order to prevent zero-effort and live minimal-effort impersonation attacks [8]. Gadaleta and Rossi developed a gait recognition based user authentication system calculating acceleration, orientation, and angular velocity features engaging convolutional neural network (CNN) and comprehending them through one class support vector machine (SVM) [9]. Zou et. al. employed a hybrid neural network architecture to confirm an individual's walk collecting the inertial sensor data from an accelerometer and gyroscope via a smartphone. The gait features were extracted through deep CNN (DCNN) maintaining time- series fashion and segregated with long short-term memory (LSTM) network [10].

On the contrary, other types of gait identification or biometric research considers image and video frames to analyse unique postural characteristics of walk such as, Wolf et. al. who created a 3D CNN for human walk identification taking gray-scale images and optical flow as the input that is invariant to clothing, walking speed, and viewing angle [11]. Tang et. al. proposed a method to overcome a limited number of gait view data assuming the 3D shape shares a common view surface. Walking image shapes were formed via the Laplacian deformation energy function inpainting gait silhouettes which were re-projected onto the 2D space to construct partial gait energy images. These partial gait view images were fed into the system for classifying the person from an arbitrary view [12]. Usually, the gait biometric algorithms operate on a single person, however walking characteristics change when the person walks with multiple persons. This was addressed by Chen et. al. computing human graphlets and integrating them into a tracking-by-detection method to obtain a person's complete silhouette. The attributes were determined using a latent conditional random field (L-CRF) model and classifying latent structural SVM framework [13]. Thapar et. al. presented another user authentication system resolving view angle issue and classifying walking patterns without human cooperation through 3D CNN model, where the first stage identifies different view angles, and second stage detects the person [14]. Battistone and Petrosino modelled a system for action and gait recognition realising structured data and temporal information through deep neural network named time based graph long short-term memory (TGLSTM) [15]. A model named PoseGait was developed by Liao et. al. extracting joint angles, limb length, joint motions and realizing through CNN to prevent the effect of illumination change and clothing on gait recognition

[16]. Zhang et. al. classified gait patterns considering canonical and pose features along with walking speed, carrying, and clothing from high resolution RGB images modelling LSTM network for biometric authentication [17]. Chai et. al. created an architecture for biometric gait recognition named gate controlled and shared attention ICDNet (GA-ICDNet) processing covariate and identity feature separately and in parallel from gait energy images [18]. Gupta presented a pose invariant gait based user authentication system extracting features from human body's silhouette of pose energy images and adapting them via generator advisory network (GAN) model [19]. Zhang et. al. proposed gait biometry applying Koopman theory, deriving features from gait silhouettes and realising them by employing convolutional variational autoencoder and deep Koopman embedding system [20].

Impulse radio ultrawideband (IR-UWB) pulsed Doppler radar is also utilized as a markerless technique by researchers because of its high bandwidth and precise performance in describing human motion [21]. However, gait is either analysed in 2D determining time–frequency variation with the help of signal processing tools from IR-UWB micro-Doppler (μD) signature [22] [23] or the region of interest (ROI) is extracted from the signatures and classified using ML to understand locomotion characteristics [24]. Recently, UWB radar sensors have been used to collect gait data from different angles and classified the fused sequence by Bi-LSTM (Bidirectional LSTM) network focusing the natural gait transition and fall events [25].

3D non-wearable or markerless gait biomechanic assessment is extremely important to provide large scale screening to prevent and treat musculoskeletal injuries, hence the proposed study is focused on 3D gait detection and recognition with wide-ranging artificial intelligence application. 3D gait representation techniques, such as marker-based approach (without ML and DL) is mainly applied by clinicians or health professionals, while markerless methods (engaging image classification with ML and DL) are predominantly practised by engineering disciplines. Hence, improved gait research requires an alternative method to rep- resent locomotion in 3D. Augmenting such systems with classification via ML or DL would bring added benefits such as assisted and automated detection and remote diagnostics/rehabilitation opportunities. The authors proposed and reported the first ever 3D model-based gait identification method from impulse radio ultra-wideband (IR-UWB) wireless communication technology applying spherical trigonometry [26], [27]. This is a markerless, nonintrusive, non-contact, and camera-less prototype where gait motion is interpreted through the understanding of anatomical reference planes. The model has been further improved in this research employing vector algebra to calculate knee angles. Simultaneously, the model has been corroborated with the popular Kinect Xbox One sensor for knee angle measurement as this is the most successful model-free gait analysis system reported by field researchers [28]–[30]. Bland and Altman (B&A) statistics has been measured between the proposed IR-UWB prototype and Kinect sensor results to verify the agreement. Finally, the proposed prototype has been incorporated with popular supervised machine learning (ML) as well as the deep neural multilayer perceptron (DMLP) techniques to investigate their potential to automatically recognize gait abnormalities with the said system. The proposed markerless prototype would permit large scale, local community based testing, not restrict patients with marker attachments and allow them to walk comfortably, more naturally and freely during diagnosis. Being easily deployable and contact free, the set-up would innately be low cost per-patient and highly scalable. The cost and inconvenience of dedicated labs, complex and single-use consumable markers could be avoided, the necessity of cleaning and potentially re-sterilization of a wearable instruments ae also avoided, and patients relieved from skin irritation as well as the potential to perform the test outside enabling social distancing requirements of the future. The model operates with very low-power which would bypass the power management issues of patches and wearables, and also this would provide a business model shift from consumable sales to a service model that provides more valuable, insightful information that could change the nature of modern gait healthcare. The detailed experimental set-up, the proposed method, result analysis, conclusion and future research direction are demonstrated in the following sections.

III. Method

A number of phases are involved in the study. Ethical clearance was required in order to conduct this research. Human participants were recruited upon acceptance of the ethical statement and examined through IR-UWB radar and Kinect Xbox sensor in an anechoic environment. Knee angles have been determined from the motion data captured using these two devices of their gait. The knee angles computed from IR-UWB radar have been fed into ML and DL after confirming its correctness comparing with Kinect's knee angles. The steps involved here are summarised and shown in Figure 2.

A. Ethical Approval Statement

Twenty-four participants have been recruited hitherto for the data collection process. Twenty participants have normal walking abilities and four participants had spasticity in this research. Full ethical approval was gained from London South Bank University, where the research code of practice and ethical guidelines are governed by the university ethics panel (UEP).

B. Laboratory & Data

A Time Domain PulsON-P410 mono-static radar module (P410-MRM) has been used to collect the non-intrusive physiological sensing phenomena reported here, shown in Figure 3a. The module is a pulsed Doppler radio transceiver that utilizes two-way time of flight (TW-TOF) omni-directional range measurement techniques. The nanosecond duration Gaussian pulses generated by the radar have low duty cycle resulting in the high pulse repetition rate (PRR) of 10 MHz enabling improved detection of human movement. The transmitting radio frequency (RF) has a center frequency at 4.3 GHz. The module adheres to FCC power restrictions for safe RF transmission.

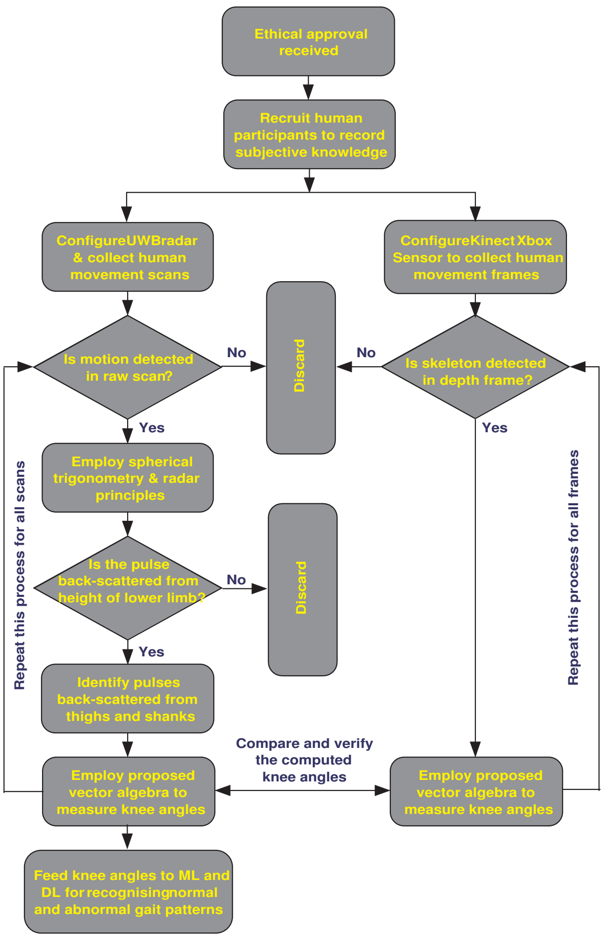

Fig. 2: Different phases involved in the proposed research.

The anechoic experimental environment is shown in Figure 3b. Initially, gender and anatomical information (height, length of the limbs) have been recorded for each individual as shown in Figure 3c.

C. Theoretical Model

To assist in the differentiation of separate body areas, azimuth and elevation angles are considered. All the ranges have been denoted here by vector notation as they have specific magnitude and direction at particular time. Figure 4a shows the elevation and azimuth angle from the received pulsed radar signal. Here, O is considered as the radar receiver, which is fixed at a point of height $\overrightarrow{OP}$ from the ground. Let, $\overrightarrow{OA}$ and $\overrightarrow{OC}$ are the range from O at time t_1 and t_2 where angle between $\overrightarrow{BC}$ and $\overrightarrow{OB}$ be α. Then the height of any movement from the ground at a particular time is h then,

$$h = |\overrightarrow{OP} - \overrightarrow{OB} \times \cos\alpha| \tag{1}$$

If the moving limb be deviates at an azimuth angle ϕ, where the travelled distances are $\overrightarrow{OA}$ and $\overrightarrow{OC}$ with specific propagation delay. Thus, the change of distance is $\overrightarrow{DA}$ at the delay interval Δt. Therefore, ϕ is calculated from the radian measure, and equivalent degree conversion is $\phi = \frac{\overrightarrow{DA} \times 360°}{\overrightarrow{OA} \times 2 \times \pi}$.

Let the coordinate of each back-scattered pulse returning from an obstacle, such as a human body, have its motion width span, distance, height from radar be denoted as a, r, h respectively. Thus each pulse can be considered a vector and represented as $a\hat{i} + r\hat{j} + h\hat{k}$ after finding the a, r, h where, $\hat{i}$, $\hat{j}$, and $\hat{k}$ are the unit vectors of 3D space. The 'a priori' properties of vector and human body have been applied further to measure the knee angles (shown in Figure 3c).

D. Knee Angles from IR-UWB Sensing

Human gait creates angles between the thigh and shank muscles during walking where the angle increases during muscle extension and decreases during flexion. This knee angle variation is significant for gait characterization. Figure 4b shows a human walking posture where the four points $\overrightarrow{L_T}$, $\overrightarrow{L_S}$, $\overrightarrow{R_T}$, $\overrightarrow{R_S} \in \mathbb{R}^3$ Euclidean space at time t, have been assumed for the thigh and shank of the left and right legs respectively. The dot product of the points from each leg provides the acute angle γ_L and γ_R between them, whereas, the measurement of the obtuse angles (β_L and β_R) are anatomically more significant. The acute left knee angles have been determined and are described in Eq. 2 considering the dot product relationship $\overrightarrow{L_T}.\overrightarrow{L_S} = |\overrightarrow{L_T}||\overrightarrow{L_S}| \cos\gamma_L$.

$$\gamma_L = \cos^{-1}\left(\frac{(a_1a_2 + r_1r_2 + h_1h_2)}{\sqrt{a_1^2 + r_1^2 + h_1^2}\sqrt{a_2^2 + r_2^2 + h_2^2}}\right) \tag{2}$$

Similarly the acute right knee angle γ_R has been calculated. Subsequently, the obtuse knee angles (β_L and β_R) for the left and right legs are $\beta_L = 180° - \gamma_L$, $\beta_R = 180° - \gamma_R$ respectively.

E. Calibration of Kinect Xbox One

The camera based Microsoft Kinect Xbox One tracks 3D human skeleton using color and depth sensors time-of-flight (TOF) technology. It has been calibrated with 30 frames per second (FPS) for color and depth sensor for video acquisition where the horizontal and vertical field views are 70° and 60°, respectively. The camera sensor operates over a range from 0.8 to 4.2 meters. It delivers 20 skeletal 3D joint coordinates at standing condition from the body posture. This skeletonization process is similar to the proposed prototype permitting the validation of the work via the Kinect. Figure 3d shows the 20 joints from a human body where, the validation process has used only 6 lower limb's joints such as, the hip left ($\overrightarrow{HL}$), knee left($\overrightarrow{KL}$), ankle left ($\overrightarrow{AL}$), hip right ($\overrightarrow{HR}$), knee right ($\overrightarrow{KR}$), and ankle right ($\overrightarrow{AR}$). Then the vector algebra has been employed on these joints to measure knee angles for both legs. Let, the vectors $\overrightarrow{HL}$, $\overrightarrow{KL}$, $\overrightarrow{AL}$, $\overrightarrow{HR}$, $\overrightarrow{KR}$, $\overrightarrow{AR} \in \mathbb{R}^n$ in Euclidean n-space. The component form of these vectors have been denoted as, $\overrightarrow{HL} = a_5\hat{i} + r_5\hat{j} + h_5\hat{k}$, $\overrightarrow{KL} = a_6\hat{i} + r_6\hat{j} + h_6\hat{k}$, $\overrightarrow{AL} = a_7\hat{i} + r_7\hat{j} + h_7\hat{k}$, $\overrightarrow{HR} = a_8\hat{i} + r_8\hat{j} + h_8\hat{k}$, $\overrightarrow{KR} = a_9\hat{i} + r_9\hat{j} + h_9\hat{k}$, and $\overrightarrow{AR} = a_{10}\hat{i} + r_{10}\hat{j} + h_{10}\hat{k}$ where, subscripts with a, r, h represents the distance from $\hat{i}$, $\hat{j}$, $\hat{k}$ planes respectively.

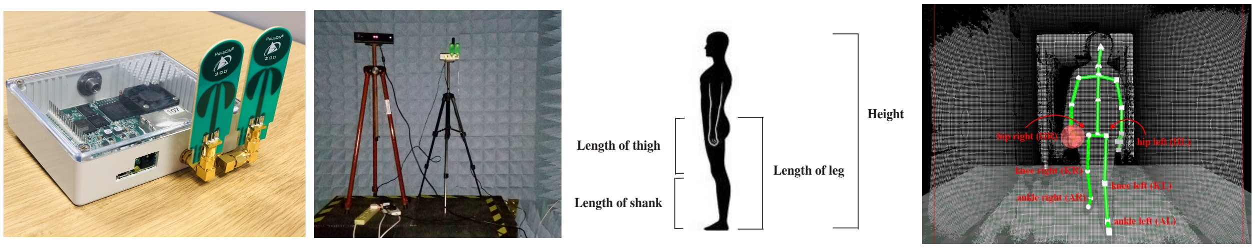

(a) UWB P410 radar module. (b) Anechoic chamber. (c) Measurement of body parts. (d) Frame from depth sensor.

Fig. 3: UWB device and the environments during data collection.

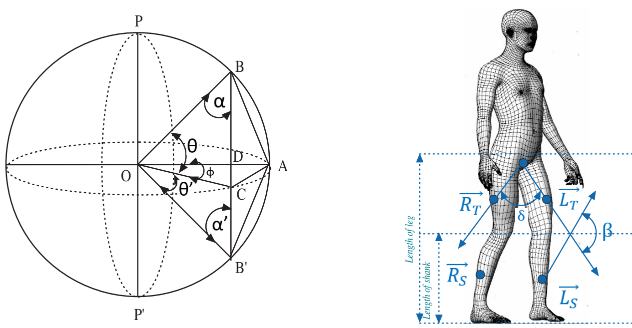

(a) Elevation and azimuth angle calculation. (b) Vectorization

Fig. 4: Three dimensional sphere consideration and vectorisation of back-scattered UWB pulse.

F. Knee angle from Kinect

The knee and ankle joints (shown in Figure 3d) from the skeletal data of both legs have been used here to calculate the two knee angles. In the case of the left leg, the connecting line between vectors $\overrightarrow{HL}$ and $\overrightarrow{KL}$ would span the vector $\overrightarrow{L_{Tk}} = a_{56}\hat{\imath} + r_{56}\hat{\jmath} + h_{56}\hat{k}$ where $a_{56} = (a_5 - a_6)$, $r_{56} = (r_5 - r_6)$, $h_{56} = (h_5 - h_6)$ and the straight line between points $\overrightarrow{KL}$ and $\overrightarrow{AL}$ would span the vector $\overrightarrow{L_{Sk}} = a_{67}\hat{\imath} + r_{67}\hat{\jmath} + h_{67}\hat{k}$ where $a_{67} = (a_6 - a_7)$, $r_{67} = (r_6 - r_7)$, $h_{67} = (h_6 - h_7)$. The dot product of $\overrightarrow{L_{Tk}}$ and $\overrightarrow{L_{Sk}}$ i.e., $\overrightarrow{L_{Tk}}.\overrightarrow{L_{Sk}} = |\overrightarrow{L_{Tk}}||\overrightarrow{L_{Sk}}| \cos\gamma'$ provides the acute angle between these two, whereas the inner knee angle would be the obtuse angle between them. The acute angle has been denoted by γ'_L and detailed in Eq. 3.

$$\gamma'_L \quad = \cos^{-1}\left(\frac{a_{56}a_{67} + r_{56}r_{67} + h_{56}h_{67}}{\sqrt{a_{56}^2 + r_{56}^2 + h_{56}^2}\sqrt{a_{67}^2 + r_{67}^2 + h_{67}^2}}\right) \quad (3)$$

Therefore, the inner knee angle or obtuse knee angle for the left leg $\beta'_L = 180° - \gamma'_L$. Similarly, the acute knee angle γ'_R between $\overrightarrow{R_{Tk}}$ and $\overrightarrow{R_{Sk}}$ for right leg has been determined where the obtuse angle or inner knee angle for right leg $\beta'_R = 180° - \gamma'_R$.

IV. Bland Altman (B&A) Plot Analysis

Differences were found between the measurements of knee angles from the IR-UWB system and Kinect, thus the outcomes have been compared using Bland and Altman (B&A) plot analysis. The B&A is a hypothetical graphical approach [31] based on the level of agreement between the two quantitative measurements by studying the mean difference and constructing limits of agreement to assess the association between methods. Let, the measured knee angles of participants from the proposed and Kinect system be k_p and k_k respectively, mean of knee angle is m_k, differences between paired knee angles is d_k, standard deviation of the differences obtained for the knee angle is s_k. The graphical approach is employed to observe the assumptions of normality of differences and other characteristics where the x-axis represents the average of measurements, and the y-axis shows the difference between the two measurements. The two systems would agree when most of the consequences lie within $d_k \pm 1.96s_k$ for the measurement of knee angle. More precisely, 95% of differences must lie within $d_k \pm 1.96s_k$ for measuring knee angles according to Bland Altman analysis. Thus, null hypothesis states here there is no significant difference between populations (measurements) taken by the proposed work and Kinect for determining the knee angles of participants where probability value $p < 0.05$ indicates acceptance of null hypothesis and correctness of assumption.

V. IR-UWB Gait Recognition Employing Machine Learning & Deep Learning

The radar module requires a propagation delay of 23.436 nanoseconds to cover the 3 meters range of the anechoic chamber testbed. Each pulse is represented by a sequence of 288 samples; thus the prototype generates (288 × 2) = 576 knee angles from each back-scattered pulse response considering the left and right leg's simultaneous movement. From the proposed work this is considered as the feature to represent normal and spastic gait to solve this two class classification problem. The knee angle's feature vector has been visualized as $\{\beta_{L_1}, \beta_{L_2}, ...\beta_{L_{288}}, \beta_{R_1}, \beta_{R_1}, ...\beta_{R_{288}}\}$, where β_L and β_R indicate the left and right knee angles respectively.

The leading non-linear classifiers such as, the k-nearest neighbour (kNN) and the support vector machine (SVM) have been implemented initially, observing the feature distribution in Euclidean hyperspace to recognize UWB gait patterns and assess the appropriateness of ML in this context. Though kNN is rudimentary it has been chosen for its simplicity as it can adapt any data without imposing a boundary structure. Flexibility is tricky because of the high variance yet this characteristic may be advantageous here. Conversely, if the data has a high variance and requires boundary structure to fit, then the SVM is selected. However, deep MLP also has been selected for its feature engineering capability that reduces the feature extraction task towards an improved classification outcome. The kNN [32] classifier has been incorporated by fine ($k\text{NN}_F$), medium ($k\text{NN}_M$), and coarse neighbourhoods ($k\text{NN}_C$) signifying 1, 3, and 5 neighbourhood numbers respectively. Two effective distance metrics, Euclidean and Mahalanobis perform well with kNN, but the Euclidean distance is considered here to measure the distance of a feature vector from its nearest neighbour to avoid the computational overhead induced by Mahalanobis, a core low overhead requirement of the system. An odd number of k has been chosen for this binary classification problem to avoid the ties in class label assignment i.e. two groups attaining the same score by the classifier. Further, SVM has also been enforced with both linear and non-linear (quadratic) kernels [33] for non-linear classification because, unlike quadratic kernel, linear kernel of SVM can also separate non-linear data in high dimensions. Subsequently, linear and quadratic kernel based SVMs have been denoted by SVML and SVMQ respectively. The state-of-art classification technique deep learning also has been studied and implemented for the gait pattern recognition task. Hence, a deep neural multilayer perceptron (DMLP) network has been designed and implemented for the classification task. The network comprises four hidden layers where the rectified linear activation function (ReLU) and cross-entropy have been employed as activation and loss function respectively. The ground truth UWB gait data information has been created during the data collection phase by observing simultaneous skeletons of participants visualized via the Kinect interface.

VI. Cross Validation & Performance Evaluation

A cross validation technique has been used to assess predictive outcomes and select models to develop SML prototypes. Model selection by cross-validation has been implemented by repeated random sub-sampling of the data, which is also known as Monte Carlo cross-validation. The dataset has been randomly partitioned to select the training (initialised with 5% data) and validation dataset (started with the rest of the 95% data). This process repeats to identify the appropriate training-testing dataset ratio and the stage of overfitting. Each model then ran for 10 rounds to acquire the appropriate ratio, subsequently the performance metrics have been aggregated and averaged over all the rounds. A number of appropriate and accepted statistical metrics such as, accuracy, sensitivity, and specificity [34] have been used to scrutinize the implemented classifiers performance.

VII. Result Analysis

The experimental results of the proposed 3D motion capture (IR-UWB) and Kinect, the subsequent conventional ML and DL execution are demonstrated in this section. Figures 5a and 5b display the front and side views of the 3D walking motion captured for one of the twenty normal walking patterns via the proposed IR-UWB response over an observation period.

The x, y, and z axis signify gait motion width, distance from radar, and height of movement respectively. Motion from the system appears like the letter 'W', displaying the symmetry of the human body with three areas labelled P_1, P_2, and P_3. Here, the area P_1 reflects the hip joint of this particular participant, P_1 to P_2 and P_1 to P_3 denote the change of position of the human body due to gait motion when one leg is lifted from

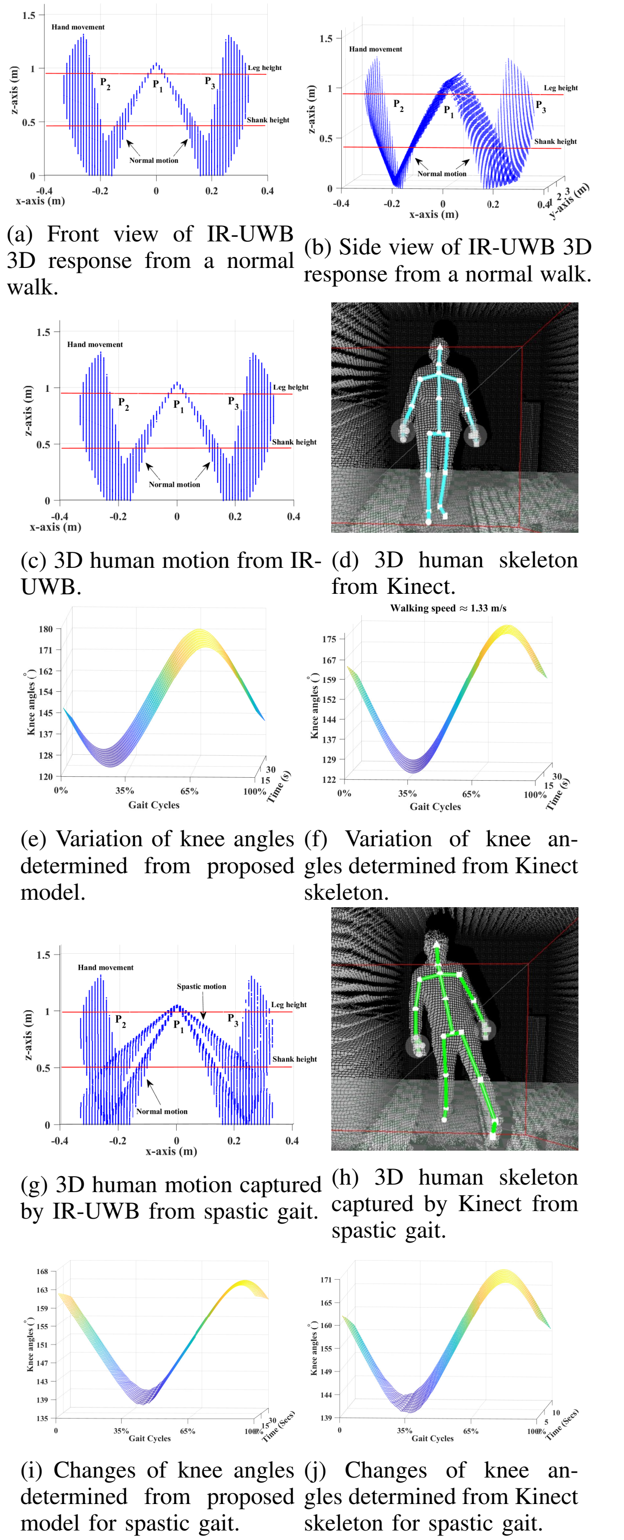

(a) Front view of IR-UWB 3D response from a normal walk.
(b) Side view of IR-UWB 3D response from a normal walk.
(c) 3D human motion from IR-UWB.
(d) 3D human skeleton from Kinect.
(e) Variation of knee angles determined from proposed model.
(f) Variation of knee angles determined from Kinect skeleton.
(g) 3D human motion captured by IR-UWB from spastic gait.
(h) 3D human skeleton captured by Kinect from spastic gait.
(i) Changes of knee angles determined from proposed model for spastic gait.
(j) Changes of knee angles determined from Kinect skeleton for spastic gait.

Fig. 5: 3D gait motion captured from proposed IR-UWB and Kinect for normal and spastic walk in anechoic environment.

the ground and the other leg makes contact with the ground to push the body forward during walking. The person walked back and forth in front of the radar (along a 3 m testbed) during the observation times, creating the distinct areas (P_1, P_2, and P_3) in 3D. The distance between the bottom of P_2 and P_3 areas represent the step base width i.e., the perpendicular distance between two steps during gait. In addition, two areas detected above leg height are the hand movements (both right and left). Figure 5c displays the front view of a walking pattern captured through the IR-UWB response and Figure 5d demonstrates the skeletonization of that same gait pattern acquired using the Kinect in the anechoic chamber.

Figure 5c shows a 3D structure resembling the letter 'W' which includes the flexion and extension of the skeletal muscle's (i.e., arm and legs) motion over time. The skeletal muscles move faster than the other body sections implying the transmission of higher energy by the bio-mechanical process enabling UWB radar to capture motion. Lower limb extension (left and right) creates a separate motion area, whereas the flexion (right and leg) of the lower limb and upper limbs creates a linear region from the shoulders further describing human motion. The person depicted in Figure 5c and 5d has an actual height of 1.55 m whereas the estimated height of the shape is 1.35 m. This is because the platform has been developed to capture all movements via the UWB up to the shoulder height from the ground level. The leg length (of the example participant) is 0.95 m and knee height of 0.45 m from the ground level have been used to separate each lower limb sections to determine the left and right knee angles. Figure 5e and 5f demonstrates the estimation of knee angles (approximately varied between 120° to 178°) from the proposed study and Kinect (approximately varied between 122° to 175°) respectively using the method of Eq. 2 and Eq. 3. The x-axis denotes the single gait cycle (in percentage) of a person by considering two consecutive steps and the process has been repeated for 30 seconds then plotted in y-axis and z-axis representing the knee angles during the observation time. The troughs here represent the angles during flexion and crest signifies the angles at the time of leg extension.

Figure 5g displays the motion of a spastic gait participant and stiffness of the left leg muscle forces the person to stretch that leg more during walking which is also reflected in the Kinect skeleton of Figure 5h. The figures show that the leg deviates more from the centre of the body during walking, resulting in the unusual knee angle variation of between 135° to 163° (in Figure 5i) and 139° to 171° (in Figure 5j), determined from the proposed prototype and Kinect respectively.

A. Bland and Altman (B&A) Plot Outcomes

Theoretical details of the Bland and Altman (B&A) plot (shown in Figure 6) is presented in section IV to support the knee angle measurement performed by the proposed model. Figure 6a and 6b display the B&A plots of knee angle measurements taken by both systems for twenty normal and four abnormal gaits respectively. The x and y axis represent the mean of two measurements and difference between the two paired measurements respectively. Both methods have some degree of error with the B&A plot indicating the relationship and agreement between these two methods for non-contact gait analysis. Figure 6a shows that the bias or mean of difference is -0.653 which signifies the second method Kinect continuously displays 0.653 degree units more than the proposed IR-UWB model and 95% of the differences are within $d_k \pm 1.96 s_k$ for knee angle measurements. In addition, Figure 6b displays the bias at -2.277 when measuring participants with abnormal gait, indicating Kinect always produces 2.277 degree units more than the proposed work for measurement of knee angles and 95% differences are within $d_k \pm 1.96 s_k$. Thus, both the cases suggest that the null hypothesis is true i.e., no significant difference between the proposed and the exemplar Kinect systems are found while measuring knee angles, and the proposed model could be easily deployed for 3D motion and gait measurement across multiple rooms for remote measurement, ad-hoc and local care deployment.

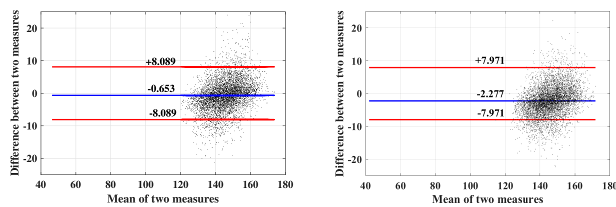

(a) B&A plot of knee angles from normal gaits. (b) B&A plot of knee angles from abnormal gaits.

Fig. 6: B&A plot of obtained knee angles experimented in anechoic chamber.

B. Machine Learning Outcomes

Training of investigated ML and DL has been initiated with 5% randomly selected data and varied up to 95%. Initially, the investigation employed the kNN classifier [32] for its simplicity and as it does not require any assumption of data distribution for decision making. Here, the k is varied from 1 to 5 and kNN k = 1 produces the highest accuracy among other NNs with 75% of training data volume. It attained a testing accuracy of 94.90% (shown in Figure 7a). The $k\mathrm{NN}_M$ produced the highest sensitivity among the three kNNs with 50% training data. Sensitivity measures the ability of the prototype to identify abnormal gait and the maximum sensitivity achieved among kNNs is 97.80% (shown in Figure 7b) in the case of k = 3. It produces fewer false positives near the decision boundary resulting in improved sensitivity over $k\mathrm{NN}_F$ and $k\mathrm{NN}_C$; also, truly positive abnormality predictions and vice versa. However, $k\mathrm{NN}_F$ achieved significant performance in the case of all three metrics, where accuracy, sensitivity, and specificity are 94.90% (shown in Figure 7a), 96.40% (shown in Figure 7b), and 92% (shown in Figure 7c). Balance between the metrics indicates that $k\mathrm{NN}_F$ can classify both normal and abnormal patterns with approximately the same high precision. Therefore, $k\mathrm{NN}_F$ demonstrates a better overall performance than the other tested NNs.

Subsequently, the SVM is investigated with two different kernel functions to acquire the hyperplane that can separate

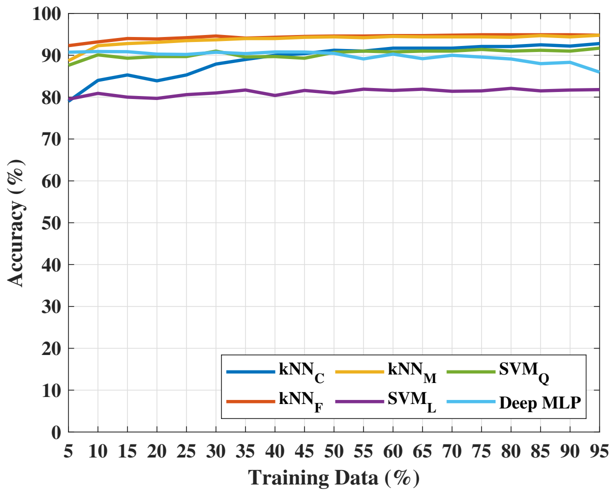

(a) Accuracy

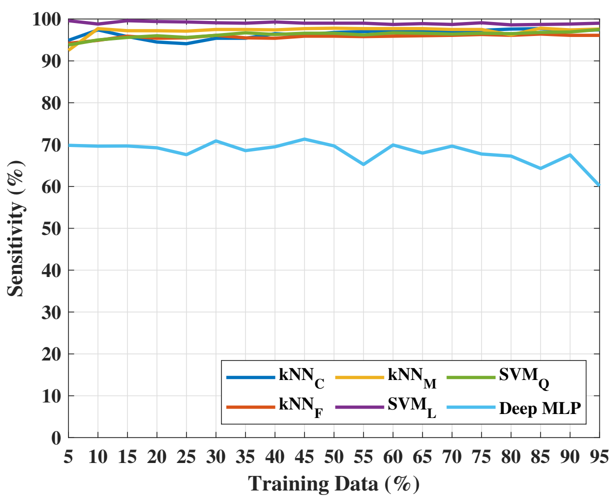

(b) Sensitivity

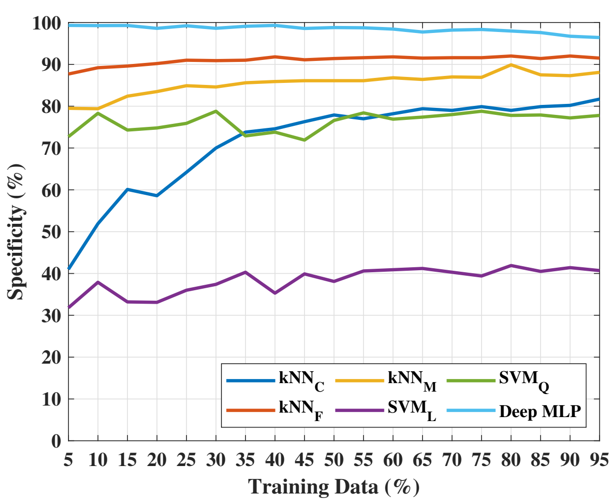

(c) Specificity

Fig. 7: Comparison of classification performance obtained from different algorithms.

participants with normal and abnormal gait patterns using the proposed UWB gait prototype. Figures 7a, 7b, and 7c show the classification results of the 2 subject types where, SVM_L and SVM_Q represent the SVMs using the linear and quadratic kernel functions respectively for prediction. SVM_L uses the optimization method, $c = \sum_i w_i k(s_i, x) + b$ where the UWB gait pattern vector x has been targeted to classify, s_i is the support vector, w_i is weight, and b is the bias. Here, the linear kernel function is k. The vector x is considered a member of the normal gait group when, $c \geq 0$, or in the abnormal gait group otherwise. This creates a hyperplane that achieved lower accuracy but better sensitivity. Among the implemented SVMs, SVM_L produces the highest sensitivity of 99.60% with 15% training data, shown in the Figure 7b, indicating an acceptable efficient performance to identify abnormal gait among both kNNs and SVMs. However, specificity is 41.90% (shown in Figure 7c) demonstrating a weaker performance in identifying persons with normal gait, though the probability in identifying abnormal gaits is better in this case. SVM_Q has been employed to obtain an improved testing accuracy to differentiate normal and abnormal gaits by minimizing the gap between two groups. The considered quadratic function is $\min_x \frac{1}{2}x^T Hx + c^T x$, where $Ax \leq b$, c is a real valued vector, H is real symmetric matrix, A is real matrix, b is a real vector, and the notation $Ax \leq b$ means that every entry of the vector A_x is less than or equal to the corresponding entry of the vector b. The quadratic programming aims to discover the vector x which could minimize that function. The cross validation has also been implemented for experiment with SVM_Q. The model creates a hyperplane to classify gait subjects and achieved maximum testing accuracy of 91.70%, where sensitivity is 97.50% and specificity is 77.80% with 95% training data (shown in Figure 7a, 7b, and 7c) to identify normal and abnormal subjects. A low number of abnormal gaits are misclassified but the low specificity implies many normal gait patterns are predicted wrongly as abnormal gaits by the SVM_Q i.e., the presence of true negatives. Thus, the low specificity reduces SVM_Q appropriateness for this study.

DMLP has been configured with four hidden layers with 288, 192, 144, and 115 neurons in first, second, third, and fourth layer respectively. Adam optimization algorithm has been employed and cross-entropy loss function has been chosen as the proposed work is a two class classification task with a regularisation parameter of 0.0001 and rectified linear (ReLU) activation function. DMLP achieved a maximum accuracy, sensitivity, and specificity of 90.90% (10% training data), 71.30% (45% training data), and 99.32% (40% training data) respectively (shown in Figures 7a, 7b, and 7c). The specificity achieved by DMLP is the highest among all the classifiers investigated here.

One issue which contributed to the high accuracy attained by most of the algorithms but resulted in a variation in the achieved sensitivity and specificity results is the skewness of the dataset, i.e., only 20% of the dataset contains abnormal UWB gait data. Concisely, $k\mathrm{NN}_C$, $k\mathrm{NN}_F$, $k\mathrm{NN}_M$, SVM_Q, and DMLP all attained high accuracy indicating greater correct predictions out of the total number of predictions. But, the

TABLE I: Comparison of gait recognition performance achieved by existing research and proposed study.

Gait Recognition Models	Accuracy/ Rank-1 Accuracy	Sensitivity	Specificity	Data Capturing Device	Focus
Wolf et. al. [11]	80.00% to 100.00%	-	-	Camera	Human identification
Tang et. al. [12]	51.40% to 95.10%	-	-	Camera	Human identification
Chen et. al. [13]	62.50% to 99.00%	-	-	Camera	Human identification
Thapar et. al. [14]	97.08% to 99.90%	-	-	Camera	Human identification
Battistone and Petrosino [15]	86.40% to 98.40%	93.70%	-	Camera	Human identification
Zhang et. al. [17]	70.40% to 99.90%	-	-	Camera	Human identification
Chai et. al. [18]	97.60%	-	-	Camera	Human identification
Gupta [19]	71.00% to 92.00%	-	-	Camera	Human identification
Zhang et. al. [20]	71.80% to 95.40%	-	-	Camera	Human identification
Proposed work	**94.90%**	**96.40%**	**91.40%**	**IR-UWB Radar**	**Gait health**

decision boundaries are biased for either normal or abnormal gaits due to the data skewness. For example, $k\mathrm{NN}_C$, $k\mathrm{NN}_F$, $k\mathrm{NN}_M$, SVM_L, and SVM_Q attained high sensitivity, signifying correct abnormal gait recognition, whereas $k\mathrm{NN}_F$ and DMLP achieved significantly higher specificity than the other algorithms indicating correct normal gait prediction. However, the proposed study aims to achieve balanced metrics (i.e., high accuracy, sensitivity, and specificity) through one of the implemented classifiers. It becomes difficult to compute the orthogonal projection between the hyperplane and sample to obtain an optimal boundary for SVMs and update weights precisely for prediction purposes for deep MLP with a disproportioned dataset. However, the kNNs, particularly $k\mathrm{NN}_F$ was not affected by the imbalance problem and is the one algorithm here that attained high scores for all the metrics. Though, $k\mathrm{NN}_F$ follows a rudimentary or "lazy" approach the simple Euclidean distance computation from the nearest neighbour performed better to separate normal and abnormal gait and was found to be more efficient than the other tested classifiers. The $k\mathrm{NN}_F$ performance demonstrates that abnormal and normal gait can be recognised based on the computed knee angles from 3D IR-UWB model even with a data imbalance situation exists.

VIII. Discussion & Conclusion

The proposed gait recognition work here is the first study to investigate normal and abnormal gait patterns contemplating walking features from a 3D gait model without the use of markers, mobile inertial sensors, and/or cameras. Camera based 3D gait recognition research concentrate mainly on person identification in different circumstances, such as distinct viewing angles, with and without backpacks, occlusion by other objects, etc. However, the proposed work focuses on employing such a system for scalable gait health purposes. Direct comparison between the performance of the proposed work and other camera-based works is difficult as they have different outcomes and testing requirements, but quantitative contrast can be made to understand the advantages of the proposed study. A comparison has been carried out and the summary shown in Table I, where most recent gait recognition studies (discussed in Section II) II) have been included with their accuracy or rank-1 accuracy, sensitivity, specificity, device used, and study focus. The accuracies of other algorithms have been reported with minimum and maximum values as found from their study. Accuracy and other metrics vary because persons are identified from different viewing angles, with or without bags, and occlusions. These studies largely rely on accuracy only (except one study here) instead of sensitivity and specificity. However, the measurement of both sensitivity (i.e., identification of person with walking problem) and specificity (i.e., identification of normal walk) are required for clinically focused gait recognition tasks. $k\mathrm{NN}_F$ attained optimal performance (at 85% training data) with accuracy, sensitivity, and specificity of 94.90%, 96.40%, and 91.40% respectively in that case, demonstrating that $k\mathrm{NN}_F$ can classify both normal and abnormal gaits effectively when considering the knee angles calculated from the 3D IR-UWB model. There are two phases involved in this work; precise knee angle calculation and classification of the persons gait based on their knee angle variation. The first phase depends upon the IR-UWB radar and the 3D model. IR-UWB radar operates with a sampling rate of 16.39 GHz and provides high resolution (9 mm approx.) time domain signals of the motion scenario. These high-resolution signals provide detailed upper and lower body (includes thigh and shank) movement information. Subsequently, the knee angles have been extracted from these signals. The second phase considers unique knee angles as features to classify normal and abnormal gait patterns. The contrast between normal and abnormal knee angles are reflected accurately in the angle calculation which assisted the recognition phase. In that case, kNN performed well and produced optimal performance with one (k=1) nearest neighbour. It has been realized that simple Euclidean distance-based classification is suitable for identifying gait patterns rather than using boundary mapping and backpropagation algorithms. Practically, the person identification studies require unique and person specific features which help recognize the relevant person and needs a large number of subjects to validate studies. Therefore, the knowledge (or, features) cannot be shared with other persons. However, in the case of the proposed work here, all the available normal gaits and their knee angles are employed to correctly classify one new normal gait pattern and all of the available abnormal gaits, and their knee angles are utilized to correctly classify one new abnormal gait. Thus, all the subjects of a group contribute to recognize a new pattern of that group. Hence, the knowledge (or knee angle features) can be shared within the subject's class. Thus, the feasibility of the study can be validated with the reported number of subjects and the performance of the proposed study is not affected even with the dataset imbalance reported here.

The proposed work demonstrates a classification approach to separate the normal and abnormal gait from 3D IR-UWB gait and motion capture model, which is a markerless, non-contact, privacy maintaining, and easily deployable system. In this study, the initially researched knee angles from IR-UWB have been employed as features to train and test the constructed model. This initial study demonstrates the feasibility of employing ML and DL to classify gait patterns, which does not include the type of gait abnormality. The participants of this study had normal or defined spastic gait characteristics. Thus, the experiment intended to classify normal and spastic gait patterns (abnormal gait group) based on knee angles, where empirically $k\text{NN}_F$ delivered optimal performance with respect to statistical performance metrics. More participants are now being recruited to establish generalized decisions regarding gait abnormality, extending this work further to identify the type of abnormality such as, spastic, scissors, propulsive, waddling, steppage gait automatically via ML. The performance may differ from present outcomes when other types of abnormal gaits are classified. The performance analysis indicates that the further work is required on the hyperplane created by nearest neighbour classifier function, thus the fine tuning of mechanisms such as, correlation of features within feature vector, distance metrics, and number of nearest neighbours would be subsequently observed.

References

[1] Michael W Whittle. *Gait analysis: an introduction*. Butterworth-Heinemann, 2014.

[2] Barbara A Gowitzke and Morris Milner. *Scientific bases of human movement*. Williams & Wilkins, 1988.

[3] Dictio. What are the symptoms of abnormal walking or gait abnormalities? https://www.dictio.id/t/apa-saja-gejala-dari-cara-berjalan-yang-tidak-normal-atau-walking-gait-abnormalities/6367, Thursday 10 November 2017. [Online; accessed 10th March, 2019].

[4] Aurelio Cappozzo, Ugo Della Croce, Alberto Leardini, and Lorenzo Chiari. Human movement analysis using stereophotogrammetry: Part 1: theoretical background. *Gait & posture*, 21(2):186–196, 2005.

[5] Elif Surer and Alper Kose. Methods and technologies for gait analysis. In *Computer Analysis of Human Behavior*, pages 105–123. Springer, 2011.

[6] Haiyan Luo, Song Ci, Dalei Wu, Nicholas Stergiou, and Ka-Chun Siu. A remote markerless human gait tracking for e-healthcare based on content-aware wireless multimedia communications. *IEEE Wireless Communications*, 17(1):44–50, 2010.

[7] Gelan Yang, Wei Tan, Huixia Jin, Tuo Zhao, and Li Tu. Review wearable sensing system for gait recognition. *Cluster Computing*, 22(2):3021–3029, 2019.

[8] Muhammad Muaaz and Rene Mayrhofer. Smartphone-based gait recognition: From authentication to imitation. *IEEE Transactions on Mobile Computing*, 16(11):3209–3221, 2017.

[9] Matteo Gadaleta and Michele Rossi. Idnet: Smartphone-based gait recognition with convolutional neural networks. *Pattern Recognition*, 74:25–37, 2018.

[10] Qin Zou, Yanling Wang, Qian Wang, Yi Zhao, and Qingquan Li. Deep learning-based gait recognition using smartphones in the wild. *IEEE Transactions on Information Forensics and Security*, 15:3197–3212, 2020.

[11] Thomas Wolf, Mohammadreza Babaee, and Gerhard Rigoll. Multi-view gait recognition using 3d convolutional neural networks. In *2016 IEEE International Conference on Image Processing (ICIP)*, pages 4165–4169. IEEE, 2016.

[12] Jin Tang, Jian Luo, Tardi Tjahjadi, and Fan Guo. Robust arbitrary-view gait recognition based on 3d partial similarity matching. *IEEE Transactions on Image Processing*, 26(1):7–22, 2016.

[13] Xin Chen, Jian Weng, Wei Lu, and Jiaming Xu. Multi-gait recognition based on attribute discovery. *IEEE transactions on pattern analysis and machine intelligence*, 40(7):1697–1710, 2017.

[14] Daksh Thapar, Aditya Nigam, Divyansh Aggarwal, and Punjal Agarwal. Vgr-net: A view invariant gait recognition network. In *2018 IEEE 4th international conference on identity, security, and behavior analysis (ISBA)*, pages 1–8. IEEE, 2018.

[15] Francesco Battistone and Alfredo Petrosino. Tglstm: A time based graph deep learning approach to gait recognition. *Pattern Recognition Letters*, 126:132–138, 2019.

[16] Rijun Liao, Shiqi Yu, Weizhi An, and Yongzhen Huang. A model-based gait recognition method with body pose and human prior knowledge. *Pattern Recognition*, 98:107069, 2020.

[17] Ziyuan Zhang, Luan Tran, Feng Liu, and Xiaoming Liu. On learning disentangled representations for gait recognition. *IEEE Transactions on Pattern Analysis and Machine Intelligence*, 2020.

[18] Tianrui Chai, Xinyu Mei, Annan Li, and Yunhong Wang. Semantically-guided disentangled representation for robust gait recognition. In *2021 IEEE International Conference on Multimedia and Expo (ICME)*, pages 1–6. IEEE, 2021.

[19] Sanjay Kumar Gupta. Reduction of covariate factors from silhouette image for robust gait recognition. *Multimedia Tools and Applications*, pages 1–26, 2021.

[20] Shaoxiong Zhang, Yunhong Wang, and Annan Li. Cross-view gait recognition with deep universal linear embeddings. In *Proceedings of the IEEE/CVF Conference on Computer Vision and Pattern Recognition*, pages 9095–9104, 2021.

[21] Joshua Chong Yue Lai, Ying Xu, Erry Gunawan, Eric Chern-Pin Chua, Arash Maskooki, Yong Liang Guan, Kay-Soon Low, Cheong Boon Soh, and Chueh-Loo Poh. Wireless sensing of human respiratory parameters by low-power ultrawideband impulse radio radar. *IEEE Transactions on Instrumentation and Measurement*, 60(3):928–938, 2010.

[22] Ann-Kathrin Seifert, Moeness G Amin, and Abdelhak M Zoubir. New analysis of radar micro-doppler gait signatures for rehabilitation and assisted living. In *2017 IEEE International Conference on Acoustics, Speech and Signal Processing (ICASSP)*, pages 4004–4008. IEEE, 2017.

[23] Yun Seo Koo, Lingyun Ren, Yazhou Wang, and Aly E Fathy. Uwb microdoppler radar for human gait analysis, tracking more than one person, and vital sign detection of moving persons. In *2013 IEEE MTT-S International Microwave Symposium Digest (MTT)*, pages 1–4. IEEE, 2013.

[24] Ghassem Mokhtari, Qing Zhang, Chad Hargrave, and Jonathon C Ralston. Non-wearable uwb sensor for human identification in smart home. *IEEE Sensors Journal*, 17(11):3332–3340, 2017.

[25] Haobo Li, Ajay Mehul, Julien Le Kernec, Sevgi Z Gurbuz, and Francesco Fioranelli. Sequential human gait classification with distributed radar sensor fusion. *IEEE Sensors Journal*, 21(6):7590–7603, 2020.

[26] S. P. Rana, M. Dey, M. Ghavami, and S. Dudley. Iterator: A 3d gait identification from ir-uwb technology. In *2019 41st Annual International Conference of the IEEE Engineering in Medicine and Biology Society (EMBC)*, pages 782–787, 2019.

[27] S. P. Rana, M. Dey, M. Ghavami, and S. Dudley. Non-contact human gait identification through ir-uwb edge-based monitoring sensor. *IEEE Sensors Journal*, 19(20):9282–9293, 2019.

[28] Jing Gao, Peishang Gu, Qing Ren, Jinde Zhang, and Xin Song. Abnormal gait recognition algorithm based on lstm-cnn fusion network. *IEEE Access*, 7:163180–163190, 2019.

[29] Saikat Chakraborty, Shaili Jain, Anup Nandy, and Gentiane Venture. Pathological gait detection based on multiple regression models using unobtrusive sensing technology. *Journal of Signal Processing Systems*, pages 1–10.

[30] Matteo Zago, Matteo Luzzago, Tommaso Marangoni, Mariolino De Cecco, Marco Tarabini, and Manuela Galli. 3d tracking of human motion using visual skeletonization and stereoscopic vision. *Frontiers in Bioengineering and Biotechnology*, 8:181, 2020.

[31] J Martin Bland and DouglasG Altman. Statistical methods for assessing agreement between two methods of clinical measurement. *The lancet*, 327(8476):307–310, 1986.

[32] Thomas M Cover, Peter Hart, et al. Nearest neighbor pattern classification. *IEEE transactions on information theory*, 13(1):21–27, 1967.

[33] Shigeo Abe. *Support vector machines for pattern classification*, volume 2. Springer, 2005.

[34] David Martin Powers. Evaluation: from precision, recall and f-measure to roc, informedness, markedness and correlation. 2011.

Soumya Prakash Rana (M'20) is a Post-Doctoral Research Fellow (fellowship co-sponsored by UBT Srl) at London South Bank University (LSBU), London, UK, working in field of application of Artificial Intelligence to microwave imaging data for breasts lesion detection and classification. He has completed his PhD from London South Bank University, London, UK and received his Bachelor (BE) and Master (MTech) Degree from The University of Burdwan and West Bengal University of Technology, India in 2009 and 2012 respectively from the Department of Computer Science and Engineering. He worked as a junior and senior research fellow (March, 2013 to August, 2016) at Jadavpur University, India on Content Based Image Retrieval. The project was funded by University Grants Commission Basic Scientific Research (UGC-BSR). His research interest includes human physiological movement and localisation from Ultra-wideband (UWB) signals, gait analysis, machine learning, big data analysis, image processing, and energy optimization in smart buildings, renewable energy technology, and Computer-aided Diagnosis using Machine Learning/AI for smart health.

Maitreyee Dey has nearly a decade of technical research experience. Her current position at Neuville aligns with a joint-Post-Doctoral Research Fellow position in the School of Engineering at London South Bank University (LSBU) under the European Regional Development Fund (ERDF) support for Low Carbon London. Prior to LSBU, Maitreyee worked as a junior research fellow (2012 – 2015) at Jadavpur University in India on automatic target recognition using FLIR imagery. Her research interests include machine learning, artificial intelligence, pattern recognition, big data analysis, energy optimization in smart buildings, renewable energy technology, and image processing.

Mohammad Ghavami is currently a Professor of telecommunications with the London South Bank University. Prior to this appointment, he was with King's College London, from 2002 to 2010, and with the Sony Computer Science Laboratories, Tokyo, from 2000 to 2002. He has authored the books, namely the Ultra-Wideband Signals and Systems, and the Adaptive Antenna Systems, and has published over 140 technical papers mainly related to UWB and its medical applications. He holds three US and one European patents. He won the esteemed European Information Society Technologies Prize, in 2005, and two invention awards from Sony. He has been the Guest Editor of the IET Proceedings Communications, the Special Issue on Ultra-Wideband Systems, and the Associate Editor of the Special Issue of the IEICE Journal on UWB Communications.

Sandra Dudley is a Professor of Communication systems and Director of Research in the School of Engineering London South Bank University, London, U.K. She received the PhD in Physics from the University of Essex, UK. Her interest in low power and remote sensing schemes has led to adaptive optical-wireless systems research and the development of smart strategies for inherent physical networks, in particular a world record with BT research on lowest power broadband systems for last mile access broadband systems. She investigates areas ranging from wireless sensor networks, remote sensing, non-wearable technology, and imaging. Augmenting that she also carries out research in data processing of the signals from such systems aiming towards complete platforms ready for upscaling. Sandra manages PhDs and Research Associates in the above areas. She collaborates and leads on a number of UK, EU and IUK research grants with applications in remote user monitoring and data processing.